Time courses of cell electroporation as revealed by submicrosecond imaging of transmembrane potential

Masahiro Hibino,* Hiroyasu Itoh,‡ and Kazuhiko Kinosita, Jr.*

*Department of Physics, Faculty of Science and Technology, Keio University, Hiyoshi, Kanagawa 223, Japan; and ‡Tsukuba Research Laboratory, Hamamatsu Photonics K. K., Tokodai, Ibaragi 300-26, Japan

ABSTRACT Changes in the membrane conductance of sea urchin eggs, during the course of electroporation, were investigated over the time range of 0.5 μs to 1 ms by imaging the transmembrane potential at a submicrosecond resolution with the voltage-sensitive fluorescent dye RH292. When a rectangular electric pulse of moderate intensity was applied across an egg, a position-dependent potential developed synchronously with the pulse, as theory predicts for a cell with an insulating membrane. From the rise and fall times, the membrane capacitance of unfertilized eggs was estimated to be 0.95 $\mu F/cm^2$ and the intracellular conductance 220 Ω · cm. Under an electric pulse of much higher intensity, the rise of the induced potential stopped at a certain level and then slowly decreased on the microsecond time scale. This saturation and subsequent reversal of the potential development was ascribed to the introduction of finite membrane conductance, or permeabilization of the membrane, by the action of the intense pulse (electroporation). Detailed analysis indicated the following: already at 0.5 μs in the rectangular electric pulse, the two sides of the egg facing the positive and negative electrodes were porated and gave a high membrane conductance in the order of 1 S/cm^2; the conductance on the positive side appeared higher. Thereafter, the conductance increased steadily, reaching the order of 10 S/cm^2 by 1 ms. This increase was faster on the negative-electrode side; by 1 ms the conductance on the negative side was more than twice that on the positive side. The recovery of the porated membrane after the pulse treatment was assessed from the membrane conductance estimated in a second electric pulse of a small amplitude. At least two recovery processes were distinguished, one with a time constant of 7 μs and the other 0.5 ms, at the end of which the membrane conductance was already <0.1 S/cm^2.

INTRODUCTION

Application of an intense electric pulse across a cell renders the cell membrane permeable to solute molecules as though aqueous pores are created in the membrane. This process, called electroporation or electropermeabilization, has been used as a tool for introducing foreign substances such as exogenous DNA into cells or, more generally, for artificially controlling intracellular compositions. Despite these widespread applications in recent years, molecular events underlying electroporation are not yet clear and are under extensive investigations (for reviews, see, e.g., references 1–4).

One difficulty in the study of electroporation mechanism is that the process of permeabilization is extremely rapid. Even a submicrosecond electric pulse, with a large enough amplitude, can cause electroporation (5). Also, the permeable state of the porated membrane is not stable: the permeability generally decreases with time, and the decrease is appreciable already in the microsecond time range (6). Analysis of the poration events thus requires a temporal resolution of a submicrosecond.

Recently we have developed a pulsed-laser fluorescence microscope with which we can record microscopic images with an exposure time of a submicrosecond (7–9). This system provides us not only with the required temporal resolution but also with the capability of observing spatial differences within a single cell. Thus, we have been able to detect, in sea urchin eggs, a rapid and local augmentation of the ionic conductance of the cell membrane while the cell was exposed to a microsecond electric pulse.

In this paper, we extend these previous studies and report detailed time courses of electroporation. As in the previous studies, we visualized the transmembrane potential in sea urchin eggs with a voltage-sensitive fluorescent dye. Theoretically, an electric field applied across a cell will induce a large transmembrane potential because the cell membrane, while intact, is effectively an insulator. When the membrane is porated and conducts ionic current, this transmembrane potential should be diminished. On this basis, we were able to infer the extent of poration, as a function of time and position in the egg, from changes in the observed potential. The major finding in this report is an asymmetry of poration: the membrane conductance on the negative-electrode side increased faster than the conductance on the positive side. Although asymmetric permeations of solute molecules into or out of electroporated cells have already been documented (10–14), our current result is the first clear demonstration of the asymmetry during, not after, the pulse treatment.

MATERIALS AND METHODS

Details of the experimental procedures have been described in reference 9. Below we present only an outline and modifications.

Samples

Unfertilized eggs were obtained from sea urchins *Hemicentrotus pulcherrimus, Temnopleurus toreumaticus, Anthocidaris crassispina,* or the sand dollar *Clypeaster japonicus.* The eggs were washed and sus-

M. Hibino's present address is Department of Applied Physics, School of Engineering, Nagoya University, Furo-cho, Chikusa-ku, Nagoya 464-01, Japan.

Address correspondence to Dr. K. Kinosita, Jr.

0006-3495/93/06/1789/12 $2.00

pended in one of the following media. Ca^{2+}-free sea water was prepared by adding 1 mM ethylenebis(oxyethylenenitrilo)tetraacetic acid (EGTA) to Ca^{2+}-free sea water (Jamarine Laboratories, Inc., Osaka, Japan). Na^+-free sea water contained 430 mM KCl, 60 mM $MgCl_2$, and 1 mM EGTA. These solutions were titrated to pH 7.8–8.0 with KOH. Isotonic low-salt media were prepared by adding a small amount of 0.55 M KCl to 0.9 M glucose containing 1 mM $MgSO_4$ and 0.1 mM tris(hydroxymethyl)-aminomethane (Tris) at pH 7.8. The jelly coat on the eggs disappeared during the washing procedure.

For staining, 1 vol of the eggs were suspended in 9 vol of a desired medium containing 2 μM RH292 [*N*-(3-(triethylammonium)propyl)-4-(4-(*p*-dibutyl-aminophenyl)butadienyl)-pyridinium dibromide, Molecular Probes, Inc., Eugene, OR]. After 1–2 min, the suspension was 10-fold diluted with the dye-free medium and subjected to fluorescence imaging.

All procedures were carried out at room temperature (22±2°C).

Fluorescence imaging

The eggs stained with RH292 were imaged under the pulsed-laser fluorescence microscope as described previously (7, 9). The laser excitation allowed imaging with an exposure time of only 0.3 μs. By synchronizing the laser pulse with the electric pulse applied to the sample, an image at a desired instant in the electric pulse was obtained. Normally, several images were acquired from one egg at 2-s intervals, each under different timing or configuration of the electric pulse.

Application of electric pulses

Electric pulses were applied to the eggs placed between a pair of rectangular platinized-platinum electrodes held in between a pair of coverglasses. In experiments with electric pulses < 100 μs, the spacing between the electrodes was set to 1 mm. When longer pulses were involved, a wider spacing of 2.5 mm was used to reduce the effect of electrode polarization (see below). The electric pulses were delivered from an arbitrary-waveform generator (model 75; Wavetek, San Diego, CA), amplified with a high-voltage amplifier (model 4015; NF Electronics Instruments Co., Ltd., Yokohama, Japan), and fed to the electrodes. The voltage and current across the sample were monitored on a digital storage oscilloscope (model DS-6121; Iwatsu Co., Ltd., Tokyo, Japan). The rise and fall times (10–90%) of the voltage pulses were 0.3 μs, and those for the current pulses were 0.2 μs.

Monitored voltage pulses were always rectangular. However, when a long electric pulse was applied to the highly conductive sea water, the sample current slowly decreased with time as electrode polarization proceeded. The magnitude of the decline relative to the initial pulse height could be considerably reduced by widening the gap between the electrodes and applying correspondingly higher voltage. To confirm that the waveform of the electric field the eggs actually experienced was rectangular, we put the tips of two platinum wires (platinized, diameter 0.3 mm) between the electrodes and monitored the voltage between the tips. At the electrode separation of 2.5 mm and applied voltage of 100 V (i.e., field intensity of 400 V/cm), the decline in the monitored voltage was <1% in 1 ms.

The electrode polarization also resulted in an undershoot of the sample current at the end of the applied pulse. Complete elimination of this undershoot turned out to be difficult. In experiments where aftereffects of an intense electric pulse were examined, we used a reversing pulse in which a positive, rectangular pulse was immediately followed by a negative pulse with the same amplitude and duration.

Image analysis

The fluorescence image of the stained egg appeared as a bright ring (see Fig. 1 *A* below) because the dye RH292 was bound by the cell membrane and only the bound dye fluoresced intensely. For quantitative analysis of the fluorescence image, a "ring profile" was calculated as described in reference 9. This is the intensity profile of the bright ring plotted against the position along the cell periphery. In this work, the intensity was calculated in steps of 10° (the entire periphery = 360°), and the values at intermediate positions were assigned by linear interpolation. All experimental profiles reported in this paper therefore have a limited angular resolution of 10°.

To eliminate the effect of slight inhomogeneities in the laser illumination and/or the dye staining, the profiles were divided by a reference profile obtained in the absence of the applied electric pulse. The final ring profile therefore represents the fractional change in fluorescence intensity at each position. Unless stated otherwise, the reference profile was calculated as the average of the first and last of a series of images obtained from one egg; the first and last images were always obtained without the electric pulse, and the agreement between the two, within the experimental variations, was confirmed in each experiment.

To eliminate the effect of shot-to-shot variations in the laser intensity, the ring profiles were further normalized so as to make the fractional change at the equator (on radii perpendicular to the field direction) zero. The rationale for this normalization, adopted in the previous studies, is that the transmembrane potential induced by the external field should be zero at the equator (see Eq. 1 below) and therefore the fluorescence change should also be zero. Because this reasoning is not always valid for porated cells, we also attempted analyses without this normalization. Where applicable, the omission is stated explicitly.

RESULTS AND DISCUSSION

Induction of transmembrane potential

Fig. 1 *A* shows the time-dependent changes in the fluorescence intensity of RH292, staining the cell membrane of a sea urchin egg, during and after the application of an electric pulse at 100 V/cm. The way these images were obtained is shown in Fig. 1 *B*. Before the pulse application, the cell periphery fluoresced relatively homogeneously as seen in Fig. 1 *A*, image *a*. When the electric field was turned on, the fluorescence on the positive-electrode side (right-hand side in the figure) became progressively brighter while the negative side became dimmer (images *b* and *c*). Upon removal of the field, the changes were reversed and the original, homogeneous image was restored (images *d*–*f*). The rising phase has been described earlier (7). Here we stress the similarity between the rise and fall times (see below).

The fluorescence intensity of RH292 changes basically linearly with the transmembrane potential (15). With sea urchin eggs, Hibino et al. (9) confirmed an approximate proportionality over a wide range exceeding physiological values, although some deviation from linearity was clearly noticeable. The fluorescence changes in Fig. 1 *A* thus reflect the changes in transmembrane potential, $\Delta\Psi$, induced by the externally applied electric pulse. An increase in the fluorescence intensity indicates an increase in $\Delta\Psi \equiv \Psi_{extracellular} - \Psi_{intracellular}$, and a reduction in the fluorescence intensity a decrease in $\Delta\Psi$ toward a negative value. Note that the sign of our $\Delta\Psi$ is opposite to the sign of physiological potentials in the usual definition.

Theoretically, the potential $\Delta\Psi$ induced by an external field E_0 is given, for a spherical cell of radius a, by

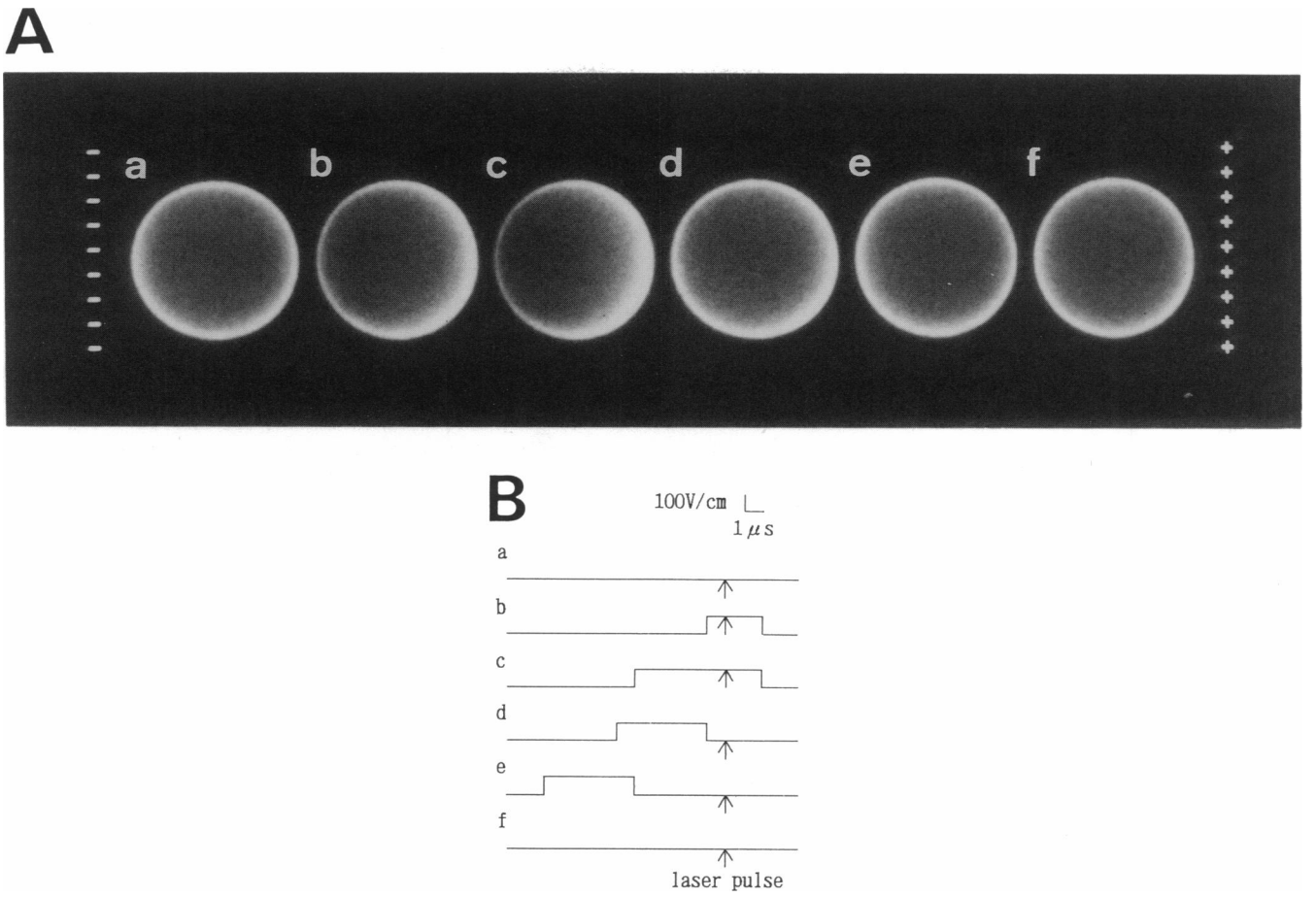

FIGURE 1 (*A*) Fluorescence images of a sea urchin egg stained with RH292. Image *a* was taken before the application of an electric pulse; images *b* and *c*, 1 and 5 μs, respectively, after a field of 100 V/cm was turned on; images *d*–*f*, 1 μs, 5 μs, and 2 s, respectively, after the field was turned off. The positive electrode was to the right of the cell and the negative electrode was to the left. Egg diameter, 100 μm. Medium, Ca^{2+}-free sea water. (*B*) Timing sequences used in obtaining the six images in *A*. The laser flashed at 2-s intervals, and each time an electric pulse shown in the figure was applied to the egg.

$$\Delta\Psi = 1.5aE_0 \cos\theta[1 - \exp(-t/\tau)] \quad (1)$$

$$\tau = aC(r_i + r_e/2), \quad (2)$$

where θ is the angle between the radius to the point of observation and the radius pointing toward the positive electrode, t is the time after the field is turned on, C is the membrane capacitance per unit area, and r_i and r_e are specific resistances of the intra- and extracellular media (16). After the field is turned off, the potential decays as

$$\Delta\Psi = 1.5aE_0 \cos\theta \exp(-t/\tau) \quad (3)$$

In Eqs. 1 and 3, we ignore the physiological (resting) potential, because it is considered to be small compared with the induced potential and since we are interested in rapid changes in $\Delta\Psi$ accompanying the pulse application. The role of the physiological potential will be discussed later.

In Figs. 2 and 3, we fit the experimental time courses of the fluorescence changes, at the positive ($\theta = 0°$) and negative ($\theta = 180°$) poles, with Eqs. 1 or 3. The positive and negative signals in each pair are well fitted with the same τ, in spite of the amplitude difference due to the nonlinearity of the dye response (the departure from linearity is larger in low-salt media, as already reported [9]). Also, the rise times in Fig. 2 and fall times in Fig. 3 agree within experimental error: 1.0 versus 1.2 μs in the Ca^{2+}-free sea water, and 4.9 versus 4.8 μs in the low-salt medium containing 5 mM KCl. These results show that the fluorescence signal closely reflects the behavior of $\Delta\Psi$. The response of the dye is completely reversible, and is sufficiently rapid both in the on and off phases.

Estimation of membrane capacitance and intracellular resistance

The rise or fall times τ above allow the estimation of the membrane capacitance per unit area, C, and the specific resistance of the intracellular medium, r_i, from Eq. 2. Using measured r_e of 20 and 1,600 Ω·cm for the high- and low-salt media and the egg radius, a, of 50 μm, we obtain $C = 0.95$ μF/cm^2 and $r_i = 220$ Ω·cm. Measure-

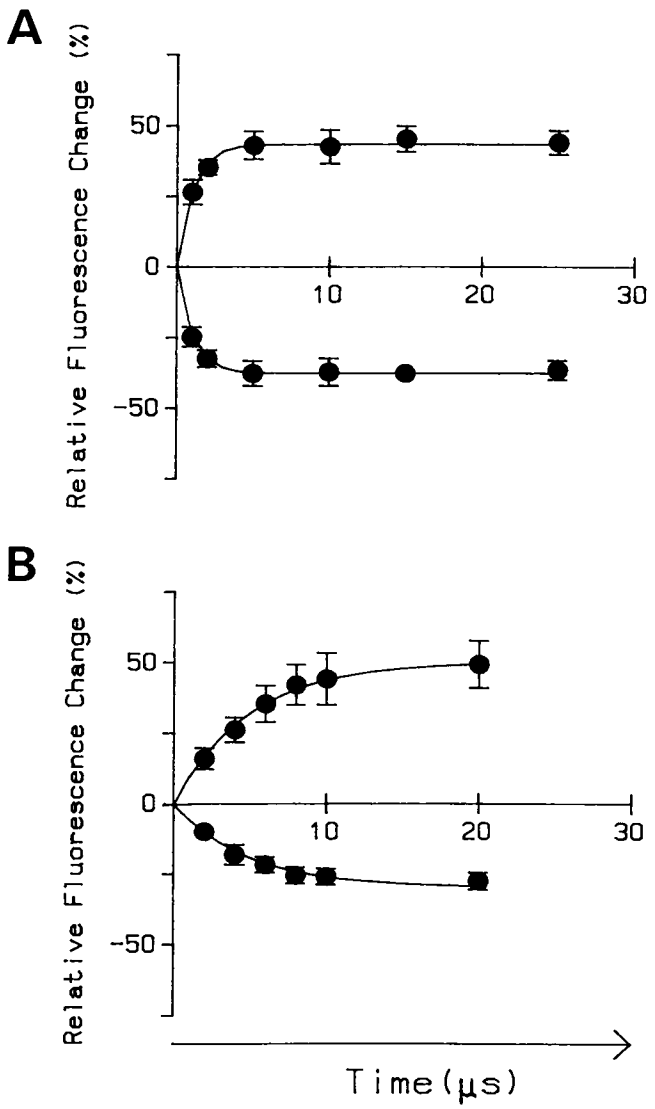

FIGURE 2 Time courses of the fluorescence change, at the positive and negative poles, induced by sudden application of an electric field of 100 V/cm; (*A*) in Ca^{2+}-free sea water; (*B*) in the low-salt medium containing 5 mM KCl. Positive changes were obtained at the pole on the positive-electrode side ($\theta = 0°$), and negative changes were obtained at the negative pole ($\theta = 180°$). Smooth lines are best-fit curves in the form of $[1 - \exp(-t/\tau)]$, where $\tau = 1.0$ μs for *A* and 4.9 μs for *B*. The experimental points (●) are the average over four eggs, the error bars showing the standard deviations. From each egg, eight images were taken at 2-s intervals, the first and last in the absence of the field; the other six were taken at the indicated timings after the onset of an electric pulse, the duration of which was 2-μs longer than each delay period. From each image taken in the pulse, a ring profile was calculated, as described in Materials and Methods, with the average of the first and last images as the reference. The profile values at $\theta = 0°$ and 180° constitute the experimental points in this figure.

ment in a low-salt medium containing 1 mM KCl (r_e = 4200 Ω · cm) gave $\tau = 10.7$ μs (data not shown), which is also consistent with the above *C* and r_e. These values for *C* and r_e are within the range of values obtained by impedance measurements on various egg suspensions (16, 17). (The estimation of *C* and r_i from τ measured with a voltage-sensitive dye was first reported by Ehrenberg et al. [18]).

Time course of electroporation

Eq. 1 suggests that $\Delta\Psi$, and therefore the fractional change in the fluorescence intensity of RH292, should be proportional to the intensity of the applied field, E_0. This was not the case for $E_0 > 100$ V/cm: under intense electric fields, the fluorescence change saturated above a

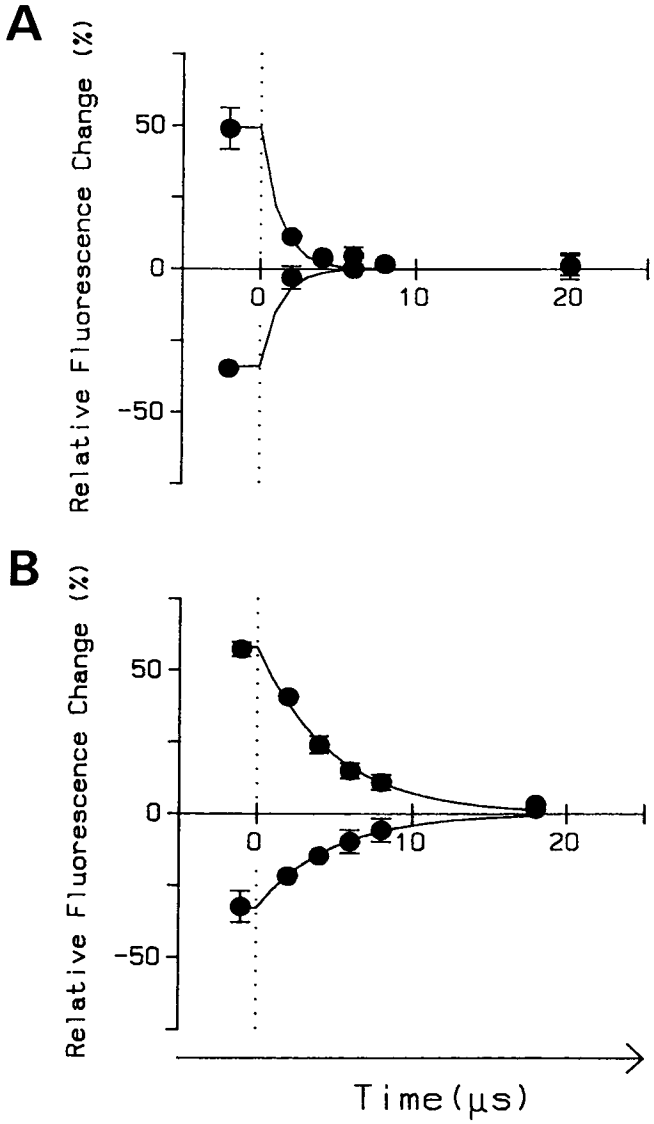

FIGURE 3 Reversal of the fluorescence change after the removal of an externally applied electric pulse. The applied pulse was a symmetrical reversing pulse, consisting of a negative-going rectangular pulse of amplitude −100 V/cm and duration of 20 μs immediately followed by a positive pulse of amplitude 100 V/cm and duration of 20 μs. The abscissa indicates the time between the end of the reversing pulse and the laser illumination; (*A*) in Ca^{2+}-free sea water; (*B*) in the low-salt medium containing 5 mM KCl. Smooth lines are exponential decays, $\exp(-t/\tau)$, where $\tau = 1.2$ μs for *A* and 4.8 μs for *B*. Experiments were made as in Fig. 2, except that all electric pulses were identical and that the images were taken after, not during, the electric pulse.

certain level (7, 9). The saturation was ascribed to electroporation: conduction of ionic current through the porated membrane prevented further increase in $\Delta\Psi$. Because $\Delta\Psi$ calculated from Eq. 1 exceeds 1 V for $E_0 >$ 133 V/cm (a = 50 μm), the saturation behavior is consistent with the reported threshold for electroporation of ~1 V for most cell membranes (1, 3), including the egg membrane of a sea urchin (19).

The extent of electroporation, or the ionic conductance of the porated membrane, can be assessed from the departure of the observed $\Delta\Psi$ from that predicted in Eq. 1. To investigate the time course of electroporation, therefore, we measured the fractional change in the fluorescence intensity at various times in an intense, rectangular electric pulse that would induce electroporation. The results are plotted in Fig. 4 *A–G* in the form of the ring profiles. The ordinate is considered to be approximately proportional to $\Delta\Psi$, and the abscissa is θ in Eq. 1 ($\theta = 0°$ at position R).

The dotted curves in the figure are the control, showing the time-dependent change of the ring profile under the applied field of 67 V/cm, for which $|\Delta\Psi|$ in Eq. 1 does not exceed 0.5 V. The dotted profiles are all approximately cosine-shaped as expected from Eq. 1. After the initial increase seen in Fig. 4, *B–D*, the amplitude of the dotted profile remains practically constant up to 1 ms. This is also consistent with Eq. 1. Apparently, there is no sign of electroporation in the dotted curves.

The solid curves in Fig. 4 were obtained under the applied field of 400 V/cm, for which the maximal $\Delta\Psi$ expected from Eq. 1 is 3 V, far above the poration threshold of ~1 V. If electroporation had not taken place, the solid profile in each panel would simply have been the sixfold magnification of the dotted profile. In fact, however, the solid profiles are depressed at the top and bottom, showing the saturation behavior. The values of $\Delta\Psi$ represented by the solid profiles may be read, approximately (but see below), by reference to the dotted profiles in Fig. 4, *D–G*, of which the top and bottom represent 0.5 and −0.5 V, respectively. On the positive-electrode side (position R), $\Delta\Psi$ apparently saturated at ~0.5 V and then slowly decreased. On the negative side (L), $|\Delta\Psi|$ initially reached ~1 V and then decreased. Poration apparently proceeded in these two regions opposing the electrodes, where $|\Delta\Psi|$ in Eq. 1 would have exceeded 1 V.

The gradual decrease in $\Delta\Psi$ indicates that the degree of poration increased on the microsecond time scale. This increase observed during the pulse application is consistent with the general tendency that the permeability of cells seconds to minutes after pulsation is higher for a longer pulse (20). An unexpected finding here is that the positive and negative sides of the solid profile changed differently, in both amplitude and form, suggesting that electroporation proceeded in an asymmetric manner. Detailed analysis is presented in the following subsections.

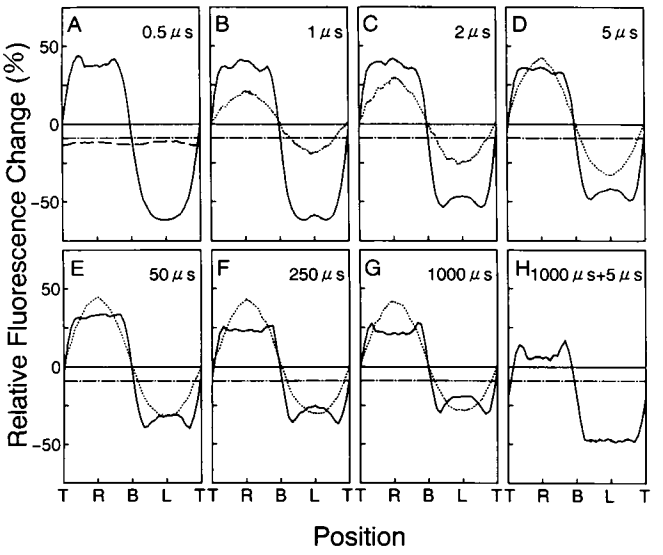

FIGURE 4 Fractional fluorescence changes in Ca^{2+}-free sea water observed at indicated time points in a rectangular electric pulse. Dotted profiles, under 67 V/cm; solid, under 400 V/cm. In *H*, two consecutive pulses were applied, first at −400 V/cm for 1 ms and then at +400 V/cm for 7 μs, and the fluorescence change was recorded at 5 μs in the second pulse. *T*, top of the image ($\theta = 90°$); *R*, right ($\theta = 0°$); *B*, bottom ($\theta = 90°$); *L*, left ($\theta = 180°$). To obtain the dotted profiles, each egg was imaged six times, the first and last in the absence of the electric pulse and second to fifth at 0.5, 1, 2, 5 μs or at 5, 50, 250, and 1,000 μs in random order. Those data in which the first and last images did not agree within experimental error were discarded. The ring profiles were calculated with the average of the first and last images as the reference and were normalized such that the profile values at *T* and *B* become zero. Each dotted profile shown here is the average over profiles obtained from 4 to 10 eggs. Solid and dashed profiles were obtained by imaging each egg five times, the first and last in the absence of the electric pulse; second at 5 μs in a 67 V/cm, 7-μs pulse; third at the indicated time in a 400 V/cm pulse; and fourth at a different time in a 400 V/cm pulse. The durations of the 400 V/cm pulses were 2 μs longer than the observation time. Those data in which the ring profile for the second image differed from the control (dotted profile in *D*) by >10% or those in which the last image showed pulse-induced dye adsorption in some part of the membrane were discarded. Each solid profile is the average, over 8–12 eggs, of the ring profiles for the third image, calculated with the first image as the reference and without normalization. The dashed profile in *A* was calculated from the fifth image in the same way; this profile is the average over all data sets used in *A–G*. The fourth images were not used because they were slightly different from the third images taken at the same time point (the egg did not fully recover between the third and fourth pulses). However, whether the amplitude of the fourth profile was larger or smaller than that of the third profile obtained from the same egg was always in accord with the tendency in *A–G*. Chain lines at −9% represent the baseline for the solid profiles (see text).

To avoid irreversible effects of the intense electric pulse at 400 V/cm, each of the solid profiles in Fig. 4 was obtained by averaging the responses of different eggs when they were exposed to the 400 V/cm pulse for the first time. The trend shown in Fig. 4, however, was also confirmed in multiple images obtained from one egg. When four images at 5, 50, 250, and 1,000 μs were taken in random order from one egg, the amplitudes of the ring

profiles always followed the decreasing order seen in Fig. 4, *D–G*, irrespective of the order of observation. The absolute magnitude of these ring profiles, on the other hand, depended on the order of observation, indicating that the egg did not recover fully during the 2-s interval between pulse applications. For example, when the image at 5 μs taken in the first pulse was compared with the 5-μs image taken after the application of a 1-ms pulse, the ring profile of the latter was lower.

Baseline of the ring profiles

Before attempting quantitative analysis, the baseline for the profiles in Fig. 4 should first be discussed. The dotted profiles have been normalized, as described in Image analysis, such that the fractional changes at the equator (*T* and *B*) are null. The dotted profiles therefore represent that part of $\Delta\Psi$ that is induced by the external field (i.e., Eq. 1). Physiological (resting) potential has to be added to obtain the total $\Delta\Psi$. The rational for the normalization is that the induced potential should be zero at the equator. This rational, however, does not necessarily apply to porated cells, because poration may well be asymmetric as the form of the solid profiles suggest. The solid profiles in Fig. 4 are therefore not normalized. They represent fractional changes relative to the initial intensity.

Now we consider that the proper baseline for the solid profiles are the chain lines in the figure for the following reasons. To obtain the solid profiles in Fig. 4, each egg was imaged five times at 2-s intervals, the first and last in the absence of applied field, second image under 67 V/cm, and third and fourth under 400 V/cm; the third image was used for the calculation of the solid profiles (see legend). When the first and last images were compared, the last image had a lower intensity as shown in the dashed curve in Fig. 4 *A*. The intensity reduction amounted to 12%. Part of this reduction is ascribed to the photobleaching of RH292 by the laser illumination. One laser pulse, on the average, reduced the intensity by 1.4%. Thus, an intensity reduction of 5.6% is expected for the last image. The additional reduction of 6% is ascribed to the disappearance of the resting potential due to electroporation. The first reason is that the depolarization is an expected consequence of electroporation: the electric current across the porated membrane should rapidly (within τ above) neutralize excess charges in the cell (9), and porated cells remain leaky to small ions for many minutes (20). In fact, fluorescence images taken 2 μs after the termination of an electric pulse of intensity 400 V/cm and duration of 1 μs already exhibited the intensity reduction (data not shown). Second, the magnitude of the additional reduction is consistent with the reported values for the resting potential of unfertilized eggs of 70–80 mV (21). Third, the additional reduction was essentially absent in the Na^+-free sea water (Fig. 5), in which the resting potential is expected to be almost

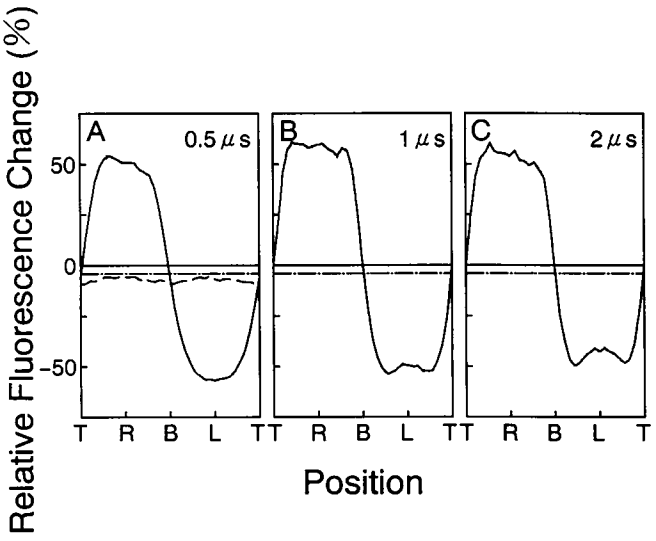

FIGURE 5 Fractional fluorescence changes under a 400 V/cm pulse in the Na^+-free sea water. See legend to Fig. 4 for details. Average over 6–14 eggs. In the Na^+-free sea water, measurements beyond 2 μs were unsuccessful because application of a 5-μs or longer pulse resulted in dye adsorption (or penetration) in the region opposing the negative electrode. Chain lines at −4% show the baseline. (The average of the dashed line is −7%, of which −5.6% is attributed to the photobleaching and the rest to the reduced resting potential. The base line is calculated as −2.8 + −1.4%.)

zero (reference 21, and K. Takemoto, unpublished data). Fourth, when several intense electric pulses were given to one egg, the large reduction in intensity took place only after the first pulse (observation under continuous illumination from a mercury lamp). Thus, for the solid profiles calculated from the third image in each experiment, the baseline (chain lines in Fig. 4) was set at −9%, −2.8% for bleaching, and −6% for the resting potential. On this baseline, $\Delta\Psi$ for the third image is zero. The difference between the solid profile and chain line therefore indicates the true $\Delta\Psi$. This $\Delta\Psi$ in Fig. 4 *A*, in particular, may include part of the resting potential, because collapse of the resting potential appeared incomplete at 0.5 μs: the application of a single pulse of duration 0.5 μs (400 V/cm) did not induce the full reduction in intensity corresponding to the total collapse of the resting potential (data not shown).

Membrane conductance of porated eggs

Having established the baseline, we now proceed to detailed analyses of Fig. 4. The degree of poration, in terms of membrane conductance, can be estimated by comparing the observed ring profiles in Fig. 4 with theoretical $\Delta\Psi$ calculated for various conductance values. Because the observed profiles suggest asymmetric poration, the membrane conductance $G(\theta)$ in the theoretical $\Delta\Psi$ is assumed to be of the following form:

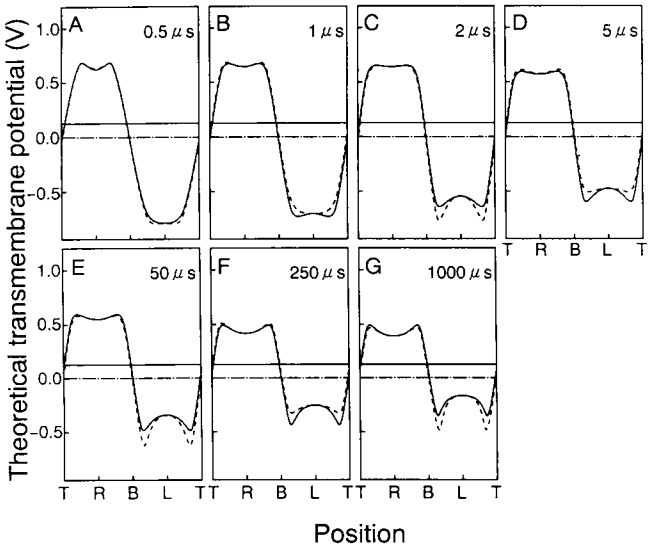

FIGURE 6 Profiles of the theoretical transmembrane potential, $\Delta\Psi \equiv \Psi_{extracellular} - \Psi_{intracellular}$, that simulate the experimental profiles in Fig. 4. Solid profiles best fit the experimental results, and dotted profiles show slight deviations. The vertical scale is chosen such that 0.5 V corresponds to the average height of dotted profiles in Fig. 4, *D–G*. For comparison with Fig. 4, the 0 V lines are shifted downward (chain lines). The parameter values, (θ_p, G_p, θ_n, G_n), where θ is in degrees and G is in S/cm^2, are, in the order of solid and dashed: *A*, (40, 1.6, 50, 0.9) and (40, 1.5, 45, 1.0); *B*, (58, 2.5, 58, 2.3) and (58, 2.6, 65, 2.1); *C*, (70, 4.2, 65, 5.2) and (70, 4.1, 60, 5.5); *D*, (70, 4.8, 65, 6.1) and (70, 4.8, 70, 5.9); *E*, (70, 5.1, 65, 8.5) and (70, 5.0, 60, 8.8); *F*, (70, 6.9, 65, 11.6) and (70, 7.0, 70, 11.3); *G*, (70, 7.5, 65, 17.7) and (70, 7.4, 60, 18.3). The ratio of the specific conductivity of the intracellular medium to that of the external sea water was taken as 0.1.

$$G(\theta) = \begin{cases} G_p \dfrac{(\cos\theta - \cos\theta_p)}{(1 - \cos\theta_p)} & (0° \le \theta \le \theta_p) \\ 0 & (\theta_p < \theta < 180° - \theta_n) \\ G_n \dfrac{(|\cos\theta| - \cos\theta_n)}{(1 - \cos\theta_n)} & (180° - \theta_n \le \theta \le 180°). \end{cases} \quad (4)$$

This $G(\theta)$, as in the previous study (9), is finite in the two regions opposing the electrodes. The conductance is maximal at the two poles, $\theta = 0°$ and $\theta = 180°$; at the positive pole, $G(\theta = 0°) = G_p$, and at the negative pole, $G(\theta = 180°) = G_n$. The particular form of $G(\theta)$ in Eq. 4 has been chosen arbitrarily, but its symmetric version ($\theta_p = \theta_n$, $G_p = G_n$) has successfully reproduced the observed ring profiles at 10–20 μs (7, 9).

Theoretical $\Delta\Psi$ for the $G(\theta)$ above was calculated as in reference 9. Curves with different parameter values (θ_p, G_p, θ_n, G_n) were generated by computer, and those that best fit the experimental curves in Fig. 4 were selected by eye. Precise fit was not pursued because the experimental profiles in Fig. 4 were rather noisy. Also, solid profiles in Fig. 4 were directly compared with the theoretical $\Delta\Psi$, ignoring the nonlinearity of the fluorescence response. The parameter values obtained should therefore be taken as gross indications of the actual $G(\theta)$. The best-fit curves are shown in solid lines in Fig. 6, and corresponding $G(\theta)$s are summarized in Fig. 7. The dependence of the theoretical $\Delta\Psi$ on the four parameters may be judged by comparing different curves in Fig. 6.

Fig. 7 shows that, under the field at 400 V/cm, both positive and negative sides of the cell were already porated at 0.5 μs (the lowest curve). This is directly indicated in the experimental profile in Fig. 4 *A*, at least for the positive side. The solid profile in Fig. 4 *A* has approximately equal heights (from the chain line) at *R* and *L*, suggesting, when the nonlinearity of the dye response is taken into account (positive changes are somewhat larger than negative changes), that the magnitude of the positive $\Delta\Psi$ at *R* was slightly smaller than the negative $\Delta\Psi$ at *L*. This difference is emphasized when we note that the resting potential, which is positive in our notation, is added to the induced potential: if the induced $\Delta\Psi$ had been symmetric, the total $\Delta\Psi$ should have been larger at *R*. The interpretation is that, already at 0.5 μs (at most 0.8 μs when the imaging time of 0.3 μs is taken into account), at least the positive side of the egg was porated and conducted appreciable current. The flat top of the solid profile at *R* in Fig. 4 *A* supports this notion.

Whether the negative side was really porated by 0.5 μs is less clear. From the measured τ of 1.1 μs above, the induced $\Delta\Psi$ in Eq. 1 at 0.5 μs in the 400 V/cm pulse is calculated to be −1.1 V at the negative pole, to which the (positive) resting potential is added. The height of the negative peak in Fig. 4 *A* is not very far from this prediction. The negative peak, however, appears relatively flat compared with a genuine cosine curve, suggesting poration. Theoretically, poration only on the positive side tends to bring $\Delta\Psi$ on the negative side toward twice the unporated value (9). This is not seen in Fig. 4 *A*, again suggesting poration also on the negative side. Thus, we consider that both sides of the cell were porated by 0.5 μs.

After 0.5 μs, the membrane conductance gradually increased with time as shown in Fig. 7. The membrane conductance eventually reached the order of 10 S/cm^2.

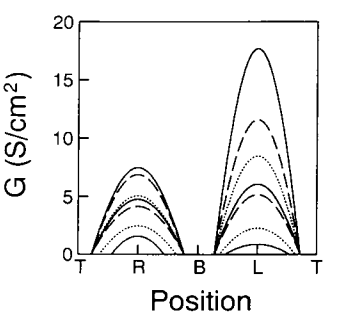

FIGURE 7 Time course of the increase in the membrane conductance, $G(\theta)$, during electroporation. Curves from bottom to top represent $G(\theta)$ at 0.5, 1, 2, 5, 50, 250, and 1,000 μs. These give the solid profiles in Fig. 6. $\theta = 0°$ at *R*, 90° at *T* and *B*, 180° at *L*.

A layer of sea water (specific conductance 50 mS/cm) with a thickness of 10 nm will have a *trans*-layer conductance of 5×10^4 S/cm^2. The membrane conductance of 10 S/cm^2 therefore corresponds to the replacement of 0.02% of the membrane area by openings filled with sea water. Or, if filled with the intracellular medium of conductance ~ 5 mS/cm, the openings would occupy ~0.2% of the membrane area.

Direct evidence for the gradual increase in membrane conductance is seen in Fig. 4, where the amplitude of the solid profile decreases with time. One could argue that the decrease might have been the result of decreasing field intensity due to electrode polarization, although this effect was shown to be negligible (see Materials and Methods). To eliminate this possibility completely, we applied an electric pulse whose intensity increased linearly from 400 to 500 V/cm during 1 ms. Even under this increasing pulse, the ring profile progressively became lower with time (5 μs to 1 ms).

One could also argue that the decrease in the profile amplitude, as well as the change in the profile shape, might have been due to changes in the property and/or location of the dye during the prolonged exposure to the intense electric field. For example, the clear depression (concavity) of the negative peak could have been due to progressive penetration of the dye molecule deeper into the membrane interior or to adsorption of free dye, both being possible causes of enhanced fluorescence. (The positive charge of RH292 makes these possibilities unlikely. Occasionally, however, extra dye adsorption at the negative pole was observed 2 s after an intense pulse treatment, raising the remote possibility of the dye adsorption during the pulse treatment.) To check these possibilities, we applied a 1-ms pulse and reversed its polarity immediately before the fluorescence measurement. The resultant profile (Fig. 4 *H*) was essentially a mirror image of the profile without reversal (Fig. 4 *G*). The deep concavity at the negative pole (*L*) in Fig. 4 *G* was preserved when the polarity was reversed to positive (*R* in Fig. 4 *H*), indicating that the concavity in fact was the result of progressive poration.

Asymmetric poration

In the induction stage, up to ~1 μs, poration on the positive side was more extensive than on the negative side. Part of the reason for this asymmetry appears to be the resting potential: as already suggested (11), $|\Delta\Psi|$ reaches the critical value for poration first on the positive side. Hence it is natural to expect that poration starts on the positive side. In the Na^+-free sea water, $\Delta\Psi$ at 0.5 and 1 μs in fact appears less asymmetric (Figs. 6, *A* and *B*).

The progress of poration was faster on the negative side (Figs. 4 and 7). Beyond 2 μs, the extent of poration on the negative side surpassed that on the positive side. Consistent with these results was the observation of selective dye permeation, after treatment with a very intense pulse (e.g., 800 V/cm for 1 ms), on the negative side: when the external medium contained RH292 or its twitterionic relative RH160, the dye molecules slowly (taking many seconds) penetrated porated eggs almost exclusively from the negative side (14). Note that RH292 is positively charged whereas RH160 is net neutral. The asymmetric penetration was not the effect of the charge of the solute.

The more extensive poration on the negative side at later times might again be ascribed to the resting potential. If poration really started on the positive side (before 0.5 μs), the current flowing through the porated area would tend to reduce $\Delta\Psi$ on the positive side while accelerating the rise in $\Delta\Psi$ on the negative side (9, 22). The speed with which $\Delta\Psi$ crosses the critical value would therefore be higher on the negative side. The damage could thus be greater on the negative side.

The resting potential, however, is at most a partial cause. In the Na^+-free sea water where the resting potential should be negligible, the ring profile started to show concavity on the negative side already at 2 μs (Fig. 5 *C*). Moreover, in this medium, too, the slow penetration of the dye molecules after the pulse treatment took place mainly on the negative side. Factors other than the resting potential are required to explain these observations. Ionic composition of the medium is also unlikely to be the dominant factor, because the dye and calcium (see below) penetration was always higher on the negative side whether the pulse treatment was made in the Ca^{2+}-free, Na^+-free, or Ca^{2+}-containing (see below) sea water, or in the low-salt media.

The major cause of the asymmetry at the later stage is probably in the structure of the cell membrane. The membrane is itself an asymmetric structure. The electric field in the membrane is directed from the extracellular to intracellular surfaces on the positive-electrode side and is reversed on the negative side. Charged components in the membrane are therefore exposed to opposite electric fields. Once pores are created, ions will flow into the membrane also in opposite directions. Thus, the direction as well as the magnitude of the electric forces on the charged components in the membrane are in general different. When the direction of the force is different, the resistance against deformation will also be different. Electroosmosis (12) may also play a part, because the flow of water through electropores on the positive and negative sides would be in opposite directions.

Apparently, the sidedness of the asymmetric dye penetration is different among different cell types. For example, with protoplasts (11) or NIH 3T3 cells (23), dye molecules entered electroporated cells predominantly from the positive-electrode side, in sharp contrast with the results on sea urchin eggs. Such a difference points to the importance of asymmetric membrane structures, which should vary among different cell types. (Sowers [12] has stressed the role of electroosmosis as the cause of asymmetric solute fluxes. Electroosmosis alone, how-

ever, cannot explain the asymmetry of slow dye permeations, because electroosmosis operates only in the presence of an electric field).

Threshold for electroporation

The poration threshold of ~1 V applies to square-wave electric pulses with a duration of the order of 10 μs. It has been shown that the threshold is a slowly decreasing function of the pulse width, both for cell membranes (5) and lipid membrane (24).

The decrease in threshold voltage was confirmed under the pulsed-laser microscope. Under the electric field at 100 V/cm, for which the maximal $\Delta\Psi$ in Eq. 1 is 0.75 V, the ring profile for RH292 fluorescence was cosine shaped in the time range around 10 μs (7, 9). When the field at 100 V/cm was applied for 1 ms, the ring profile was clearly depressed at the top and bottom, indicating poration (data not shown).

Recovery of low membrane conductance after electroporation

Previous studies (7, 9) have indicated that the membrane conductance of electroporated eggs rapidly decreases after the applied field is removed. To investigate the details of the recovery process, we made double-pulse experiments shown in Fig. 8 *A*: the aftereffect of an intense pulse (main pulse) that caused electroporation was examined by applying a second pulse of moderate intensity (monitor pulse) and observing the fluorescence response during this monitor pulse (traces *c* or *d* in Fig. 8 *A*). If the membrane remained leaky to ions, the ring profile for the monitor pulse would be low, whereas, if the recovery was complete, the profile would be indistinguishable from the profile for an unporated egg. The main pulse in these experiments was given in the form of a reversing pulse for the technical reason: as mentioned in Materials and Methods, a unidirectional pulse produced a current undershoot due to electrode polarization, which interfered with the measurement during the small monitor pulse (the undershoot indicates the presence of a residual electric field in the medium).

In Fig. 8 *B*, the fractional fluorescence changes measured at the arrows in Fig. 8 *A* are plotted. Because the main pulse was a reversing pulse, the ring profiles in these experiments were assumed to be symmetric, and their four quadrants were averaged into one. (Note that, for a pulse duration of tens of μs, the ring profile was approximately symmetric even for a unidirectional pulse; see Fig. 4). To compare the fluorescence signals observed under different field intensities (traces b–e versus *f* and *g* in Fig. 8 *A*), the observed fractional changes, which are expected to be approximately proportional to $\Delta\Psi$, were divided by aE_0, *a* being the egg radius and E_0 the field intensity, and plotted on the same graph. The ordinate in Fig. 8 *B* is scaled such that it represents $\Delta\Psi/aE_0$ (see Eq. 1), by assigning the value 1.5 to the maximal fluorescence change observed in unporated eggs (trace *b* in Fig. 8 *A*).

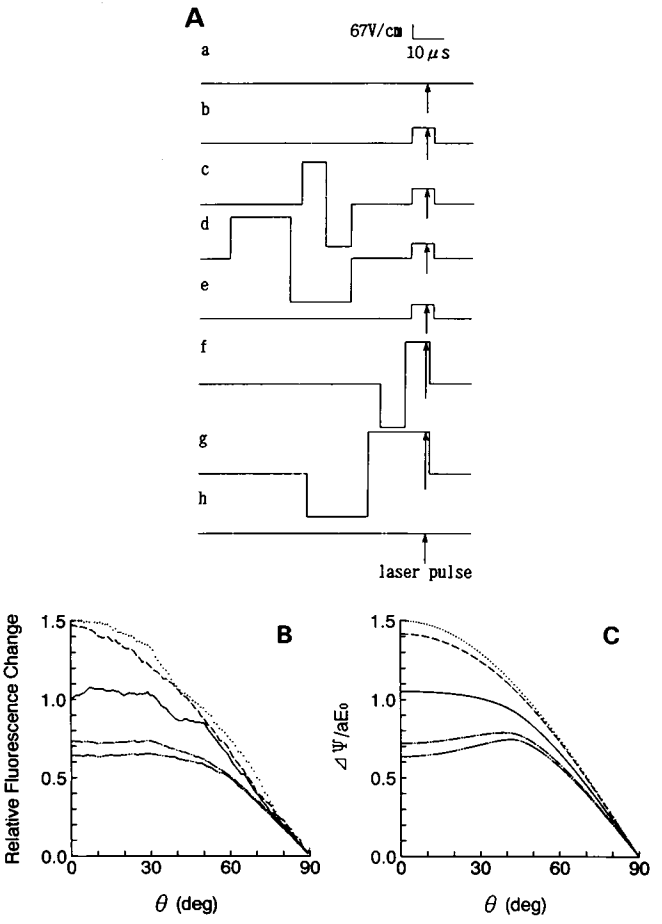

FIGURE 8 Fractional fluorescence changes observed in double pulse experiments. (*A*) Configurations of the applied electric pulses. Each egg was exposed to the eight pulse sequences at 2-s intervals, and images were taken at the arrows. The small monitor pulses in traces *b–e* had an amplitude of 67 V/cm and duration 7 μs, and observation was made at 5 μs. The main pulses in traces *c*, *d*, *f*, and *g* were reversing pulses at ±186 V/cm with duration either 8 + 8 or 20 + 20 μs. Medium was Ca^{2+}-free sea water. (*B*) Observed fractional changes. The ring profiles for traces *b–g* in *A* were calculated with the average of *a* and *h* as the reference and were normalized at the equator. Data from four eggs were averaged. Each profile was assumed to be symmetric and was further averaged over the four quadrants. Dotted profile, trace *b* in *A*; dashed, *c*; solid, *d*; chain, *f*; double chain, *g*. The profiles under 186 V/cm (chain and double chain lines) have been multiplied by 67/186, and the top of the dotted profile, obtained before poration, was assigned the ordinate value of 1.5; the ordinate therefore represents approximately $\Delta\Psi/aE_0$ (see text). *C*, theoretical $\Delta\Psi/aE_0$ that simulate the data in *B*. θ_p and θ_n in Eq. 4 were both set to 44°, and the value of $G_p = G_n$ that best fit the experimental profile was searched by trial and error. $G_p = G_n = 0$ (*dotted*), 0.1 (*dashed*), 0.7 (*solid*), 1.7 (*chain*), and 2.1 (*double chain*) S/cm². The ratio of the specific conductivity of the intracellular medium to that of the external sea water was taken as 0.1.

In Fig. 8 *B*, the dotted curve shows the ring profile for the unporated eggs. The single and double chain lines are the profiles in the main pulse of different durations (Fig. 8 *A*, traces *f* and *g*); both these curves have a low and flat top, indicative of electroporation. Corresponding pro-

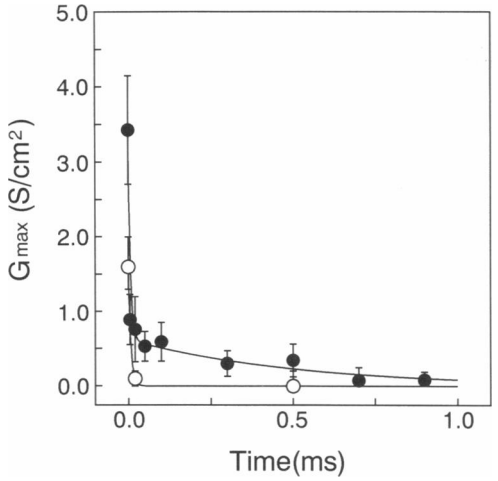

FIGURE 9 Time courses of the recovery of porated membrane. The maximal membrane conductance estimated in the monitor pulse in the double-pulse experiments is plotted against the time interval between the main and monitor pulses; the point at time 0 was taken in the main pulse. The main pulse was a reversing pulse of 20 + 20 μs (●) or 8 + 8 μs (○) at 186 V/cm, and the monitor pulse was 67 V/cm. Each egg was imaged six times, as in traces in Fig. 8 *A* in the order of *a*, *b*, *d* (●) or *c* (○), twice with different intervals, and then *g* (●) or *f* (○), and finally *h*. The maximal membrane conductance ($G_p = G_n$) was estimated as in Fig. 8 *C*. Results from 4 to 11 eggs were averaged, the error bars showing standard deviations. The smooth line connecting the closed circles represents $G = 2.8\exp(-t/7\ \mu s) + 0.6\exp(-t/500\ \mu s)$, and the line for open circles represents $G = 1.6\exp(-t/7\ \mu s)$.

files in the monitor pulse are shown in dashed and solid curves in Fig. 8 *B* (traces *c* and *d* in Fig. 8 *A*); the heights of these curves are intermediate between the unporated (dotted) and fully porated (chain) ones, indicating partial recovery of the membrane during the 20-μs interval between the main and monitor pulses. Fig. 8 *C* shows theoretical profiles that simulate the observed profiles in *B*. The simulation suggests that the membrane conductance once augmented to $G_p = G_n$ of ~2 S/cm² during the main pulse was reduced by an order of magnitude during the 20-μs interval. The recovery was slower for the longer main pulse, amplifying the relatively small difference in the membrane conductance at the end of the main pulse. This result is consistent with the tendency that larger pores remain after treatment with a longer pulse (20).

Time course of the recovery

The time courses of the membrane recovery, after the reversing main pulse at 186 V/cm for 20 + 20 μs (●) or 8 + 8 μs (○), are shown in Fig. 9, where the maximal membrane conductance ($G_p = G_n$) estimated by the curve-fitting procedure is plotted against the interval between the main and monitor pulses. The recovery after the 20 + 20 μs pulse is approximated by two exponentials, one time constant being 7 μs and the other 500 μs. By 1 ms the membrane conductance was reduced by more than an order of magnitude. At 2 s, the ring profile for the monitor pulse was no longer distinguishable from that without the main pulse. The recovery after the 8 + 8 μs pulse was fast and could not be resolved into two exponentials. The single time constant of 7 μs for the 8 + 8 μs pulse is similar to the shorter of the two time constants for the 20 + 20 μs pulse.

The shorter time constant of 7 μs is of the same order of magnitude as the one for the resealing of lipid bilayers (25). Chernomordik et al. (26) reported that, both for lipid bilayers and cell membranes, the recovery consists of at least two stages, one in microseconds and the other seconds to minutes. In erythrocyte membranes, the recovery process involved many time constants ranging from microseconds to minutes (6, 20). Obviously the recovery is not a simple exponential process, and the two time constants we report here represent only the initial phase. This initial recovery in the microsecond range is quite significant, amounting to a reduction in membrane conductance by more than an order of magnitude. Yet this fast phase alone does not lead to a complete recovery.

Recently, Chang and Reese (27) for the first time observed clear structural changes accompanying electroporation: volcano-shaped openings with diameters 20–120 nm were revealed, by rapid-freezing electron microscopy, in erythrocyte membranes exposed to an intense electric pulse. Detectable openings appeared 3 ms after the pulse, and then their size as well as number increased in the next 20 ms, and finally the openings started to shrink after several seconds. This time course is in apparent contradiction with our results above: the membrane conductance started to decrease immediately after the pulse, and significant reduction was achieved in the microsecond range. Conductance of erythrocyte membranes also behaved similarly (6). The discrepancy might not be serious, because small pores undetectable in electron microscopy can contribute to the membrane conductance, as Chang and Reese (27) pointed out. The small pores may coalesce into the large openings over milliseconds, or some of the small pores may slowly grow in size while most others rapidly shrink and close. We, however, are not sure if such processes took place also in our samples, in view of the marked difference between the two kinetics: the reduction in the membrane conductance is large and rapid, whereas the expansion of the volcano-shaped openings is delayed and slow. Parallel experiments using the same sample are desirable.

Calcium influx and fertilization envelope

The experiments in Figs. 4 and 8 were done in the Ca^{2+}-free sea water because otherwise, Ca^{2+} influx into the porated egg would lead to partial elevation of the fertilization envelope (10, 19). After a relatively mild pulse treatment, e.g., at 400 V/cm for 100 μs, in a Ca^{2+}-containing sea water, the envelope is formed mainly on the

negative side (9, 28). This is consistent with the asymmetry of membrane conductance and dye permeation described above.

A more intense pulse, e.g., at 400 V/cm for 400 μs, produces a partial envelope on the positive side, or on both sides but a larger one on the positive side (10, 13). An explanation for this has been found by time-resolved imaging of the intracellular Ca^{2+} concentration using the fluorescent probe indo-1 (13): two transient Ca^{2+} influxes were observed, an early influx from the positive side lasting a few seconds and a slower but more extensive influx from the negative side lasting tens of seconds. It appeared that the envelope on the positive side became larger when the magnitude of the early influx from the positive side was high enough to elevate the envelope over a wide area on the positive hemisphere.

The different time courses of the two Ca^{2+} influxes above imply that the recovery of the membrane was much slower on the negative side. The asymmetry during the pulse treatment, in the form of a greater membrane conductance on the negative side, is amplified by the slower recovery. The dye penetration almost exclusively from the negative side (14) may well be the result of this amplification. Slower recovery on the negative side was also indicated by the following experiment: eggs in the Ca^{2+}-free sea water were treated with an intense electric pulse and, 2 min later, the surrounding medium was replaced with the normal sea water. Then, most of the eggs produced a partial fertilization envelope on the negative side. (That the membrane remained leaky to Ca^{2+} as long as 2 min in this experiment suggests that complete recovery of the membrane may require the presence of Ca^{2+} in the medium.)

The Ca^{2+} imaging above also showed that the rise of the early influx from the positive side was much faster than the rise of the influx from the negative side. We consider that this difference is explained, at least partially, by the electrophoretic accumulation of Ca^{2+} under that part of the egg membrane that opposed the positive electrode. Under a 400 V/cm, 400 μs pulse, the maximal membrane conductance on the positive side is ~5 S/cm^2 (Fig. 7). For $\Delta\Psi$ of ~0.4 V (Fig. 4), the membrane current will, on the average, be ~1 A/cm^2, which will carry $\sim 4 \times 10^{-8}$ C during 400 μs across the porated area of $\sim 1 \times 10^{-4}$ cm^2. If 2% of the charge is carried by Ca^{2+} flowing into the egg, a total of ~4 fmol of Ca^{2+} will be accumulated beneath the membrane. (A similar value was reported by Rossignol et al. [10], who measured the total amount of Ca^{2+} taken up by an egg porated at 1 kV/cm for 100 μs). This accumulated Ca^{2+} will not be resolved in the fluorescence image, because the penetration depth should be <1 μm (mobility of Ca^{2+} in water ~ 6×10^{-4} cm$^2 \cdot$ s$^{-1} \cdot$ V^{-1}, and the field intensity outside the membrane < 400 V/cm). The fluorescence will change when the accumulated Ca^{2+} starts to spread by diffusion. After diffusion into a layer of thickness 10 μm (taking a fraction of a second), the Ca^{2+} concentration will be ~40 μM. Although this value is greater than the observed concentration of the order of 1 μM, the difference can easily be explained by the existence of efficient Ca^{2+}-sequestering systems in the egg, which eventually absorbed most of the Ca^{2+} of extracellular origin (13).

The electrophoretic accumulation above, though in a thin layer, can make a large contribution to the observed Ca^{2+} influx, because the accumulation precedes the rapid recovery of the porated membrane in the microsecond range shown in Fig. 9. On the negative side where the accumulation is not expected, Ca^{2+} will flow into the egg by diffusion through the recovering membrane. The influx will therefore be slow. An additional reason for the slower rise of Ca^{2+} influx from the negative side could be the electrophoretic depletion of Ca^{2+} from the egg surface opposing the negative electrode (10). The current that goes round the cell does not induce depletion but, once the negative side is porated, the current flowing out of the porated region will carry Ca^{2+} away. The preceding discussion, however, suggests that the depletion should be limited in a layer of thickness < 1 μm. The effect of depletion therefore cannot be the dominant cause of the slow Ca^{2+} entry from the negative side.

CONCLUSION

The pulsed-laser fluorescence microscope, which allows imaging at a submicrosecond resolution, has been shown to be a useful tool in the analysis of electroporation kinetics. The major finding in this study, the development of asymmetry during the course of electroporation, was a consequence of the combined spatial and temporal resolutions.

We do not yet understand the cause of the asymmetry. Because the dominant factor may well reside in the membrane structure, comparison among different cell types, under identical or similar conditions, should give some clue. Artificial systems of defined compositions, such as liposomes, will be particularly useful in this respect.

To fully understand the mechanism of electroporation, kinetic studies should be combined with structural studies at molecular resolution. Improvement in temporal resolution, e.g., electron microscopic detection of structural changes during pulse treatment, is highly hoped for.

We thank Dr. A. Ikegami (Keio University), Dr. Y. Inoue (RIKEN) and Dr. T. Hayakawa (Hamamatsu Photonics, K. K.) for their continuous support on which this work is based. Dr. T. Kouyama (RIKEN) allowed us to use his instruments. Dr. K. Takemoto (Hamamatsu Photonics K. K.) kindly communicated unpublished results to us. We also thank Drs. K. Hirano (Hamamatsu Photonics K. K.), S. Nemoto and M. Yamaguchi (Ochanomizu University), I. Yasumasu (Waseda University), and Y. Hamaguchi (Tokyo Institute of Technology) for valuable suggestions and the help in obtaining sea urchins, and Mr. M. Hosoda (Hamamatsu Photonics K. K.) for extensive support in developing the image-analysis system.

This work was supported by Grants-in-Aid from Ministry of Education, Science and Culture of Japan, and by Special Coordination Funds for Promoting Science and Technology from the Agency of Science and Technology.

Received for publication 30 November 1992 and in final form 23 February 1993.

REFERENCES

1. Zimmermann, U. 1982. Electric field-mediated fusion and related electrical phenomena. *Biochim. Biophys. Acta.* 694:227–277.
2. Neumann, E., A. E. Sowers, and C. A. Jordan, editors. 1989. Electroporation and Electrofusion in Cell Biology. Plenum Publishing Corp., New York.
3. Tsong, T. Y. 1991. Electroporation of cell membranes. *Biophys. J.* 60:297–306.
4. Chang, D. C., B. M. Chassy, J. A. Saunders, and A. E. Sowers, editors. 1992. Guide to Electroporation and Electrofusion. Academic Press, New York.
5. Kinosita, K., Jr., and T. Y. Tsong. 1977. Voltage-induced pore formation and hemolysis of human erythrocytes. *Biochim. Biophys. Acta.* 471:227–242.
6. Kinosita, K., Jr., and T. Y. Tsong. 1979. Voltage-induced conductance in human erythrocyte membranes. *Biochim. Biophys. Acta.* 554:479–497.
7. Kinosita, K., Jr., I. Ashikawa, N. Saita, H. Yoshimura, H. Itoh, K. Nagayama, and A. Ikegami. 1988. Electroporation of cell membrane visualized under a pulsed-laser fluorescence microscope. *Biophys. J.* 53:1015–1019.
8. Itoh, H., M. Hibino, M. Shigemori, M. Koishi, A. Takahashi, T. Hayakawa, and K. Kinosita, Jr. 1990. Multi-shot pulsed laser fluorescence microscope system. *Proc. SPIE (Soc. Photo-Optical Instrumentation Eng.).* 1204:49–53.
9. Hibino, M., M. Shigemori, H. Itoh, K. Nagayama, and K. Kinosita, Jr. 1991. Membrane conductance of an electroporated cell analyzed by submicrosecond imaging of transmembrane potential. *Biophys. J.* 59:209–220.
10. Rossignol, D. P., G. L. Decker, W. J. Lennarz, T. Y. Tsong, and J. Teissie. 1983. Introduction of calcium-dependent, localized cortical granule breakdown in sea-urchin eggs by voltage pulsation. *Biochim. Biophys. Acta.* 763:346–355.
11. Mehrle, W., U. Zimmermann, and R. Hampp. 1985. Evidence for asymmetrical uptake of fluorescent dyes through electro-permeabilized membranes of *Avena* mesophyll protoplasts. *FEBS (Fed. Eur. Biochem. Soc.) Lett.* 185:89–94.
12. Sowers, A. E. 1988. Fusion events and nonfusion contents mixing events induced in erythrocyte ghosts by an electric pulse. *Biophys. J.* 54:619–626.
13. Kinosita, K., Jr., H. Itoh, S. Ishiwata, K. Hirano, T. Nishizaka, and T. Hayakawa. 1991. Dual-view microscopy with a single camera. Real-time imaging of molecular orientations and calcium. *J. Cell Biol.* 115:67–73.
14. Kinosita, K., Jr., M. Hibino, H. Itoh, M. Shigemori, K. Hirano, Y, Kirino, and T. Hayakawa. 1992. Events of membrane electroporation visualized on a time scale from microsecond to seconds. In Guide to Electroporation and Electrofusion. D. C. Chang, B. M. Chassy, J. A. Saunders, and A. E. Sowers, editors. Academic Press, New York. 29–46.
15. Grinvald, A., R. Hildesheim, I. C. Farber, and L. Anglister. 1982. Improved fluorescent probes for the measurement of rapid changes in membrane potential. *Biophys. J.* 39:301–308.
16. Cole, K. S. 1972. Membranes, Ions and Impulses. University of California Press, Berkeley, CA. 569 pp.
17. Hiramoto, Y. 1959. Electric properties of Echinoderm eggs. *Embryologia.* 4:219–235.
18. Ehrenberg, B., D. L. Farkas, E. N. Fluhler, Z. Lojewska, and L. M. Loew. 1987. Membrane potential induced by external electric field pulses can be followed with a potentiometric dye. *Biophys. J.* 51:833–837.
19. Baker, P. F., D. E. Knight, and M. J. Whitaker. 1980. The relation between ionized calcium and cortical granule exocytosis in eggs of the sea urchin Echinus esculentus. *Proc. R. Soc. Lond. B. Biol. Sci.* 207:149–161.
20. Kinosita, K., Jr., and T. Y. Tsong. 1977. Formation and resealing of pores of controlled sizes in human erythrocyte membrane. *Nature (Lond.).* 268:438–441.
21. Chambers, E. L., and J. de Armendi. 1979. Membrane potential, action potential and activation potential of eggs of the sea urchin, *Lytechinus Variegatus. Exp. Cell Res.* 122:203–218.
22. Saulis, G., and M. S. Venslauskas. 1988. Asymmetrical electrical breakdown of the cells. Theory of phenomenon. *Stud. Biophys.* 128:155–161.
23. Tekle, E., R. D. Astumian, and P. B. Chock. 1991. Electroporation by using bipolar oscillating electric field: An improved method for DNA transfection of NIH 3T3 cells. *Proc. Natl. Acad. Sci. USA.* 88:4230–4234.
24. Benz, R., and U. Zimmermann. 1980. Pulse-length dependence of the electrical breakdown in lipid bilayer membranes. *Biochim. Biophys. Acta.* 597:637–642.
25. Benz, R., and U. Zimmermann. 1981. The resealing process of lipid bilayers after reversible electrical breakdown. *Biochim. Biophys. Acta.* 640:169–178.
26. Chernomordik, L. V., S. I. Sukharev, S. V. Popov, V. F. Pastushenko, A. V. Sokirko, I. G. Abidor, and Y. A. Chizmadzhev. 1987. The electrical breakdown of cell and lipid membranes: the similarity of phenomenologies. *Biochim. Biophys. Acta.* 902:360–373.
27. Chang, D. C., and T. S. Reese. 1990. Changes in membrane structure induced by electroporation as revealed by rapid-freezing electron microscopy. *Biophys. J.* 58:1–12.
28. Millonig, G. 1969. Fine structure analysis of the cortical reaction in the sea urchin egg: after normal fertilization and after electric induction. *J. Submicrosc. Cytol.* 1:69–84.